Saudi Pharmaceutical Journal (2016) **24**, 588–599

King Saud University

Saudi Pharmaceutical Journal

www.ksu.edu.sa
www.sciencedirect.com

ORIGINAL ARTICLE

Development and statistical optimization of nefopam hydrochloride loaded nanospheres for neuropathic pain using Box–Behnken design

S. Sukhbir [a,b,*], **S. Yashpal** [c], **A. Sandeep** [b]

[a] *Department of Research, Innovation and Consultancy, Punjab Technical University, Jalandhar-Kapurthala Highway, Kapurthala 144603, Punjab, India*
[b] *Chitkara College of Pharmacy, Chitkara University, Chandigarh Patiala National-Highway (NH-64), Rajpura, Patiala 140401, Punjab, India*
[c] *Lord Shiva College of Pharmacy, Sirsa 125055, Haryana, India*

Received 27 February 2015; accepted 15 March 2015
Available online 25 March 2015

KEYWORDS

Nefopam hydrochloride;
Neuropathic pain;
Box–Behnken design;
Solvent diffusion

Abstract Nefopam hydrochloride (NFH) is a non-opioid centrally acting analgesic drug used to treat chronic condition such as neuropathic pain. In current research, sustained release nefopam hydrochloride loaded nanospheres (NFH-NS) were auspiciously synthesized using binary mixture of eudragit RL 100 and RS 100 with sorbitan monooleate as surfactant by quasi solvent diffusion technique and optimized by 3^5 Box–Behnken designs to evaluate the effects of process and formulation variables. Fourier transform infrared spectroscopy (FTIR), differential scanning calorimetric (DSC) and X-ray diffraction (XRD) affirmed absence of drug–polymer incompatibility and confirmed formation of nanospheres. Desirability function scrutinized by design-expert software for optimized formulation was 0.920. Optimized batch of NFH-NS had mean particle size 328.36 nm ± 2.23, % entrapment efficiency (% EE) 84.97 ± 1.23, % process yield 83.60 ± 1.31 and % drug loading (% DL) 21.41 ± 0.89. Dynamic light scattering (DLS), zeta potential analysis and scanning electron microscopy (SEM) validated size, charge and shape of nanospheres, respectively. *In-vitro* drug release study revealed biphasic release pattern from optimized nanospheres.

* Corresponding author. Address: Chitkara College of Pharmacy, Chitkara University, Chandigarh Patiala National-Highway (NH-64), Rajpura, Patiala 140401, Punjab, India. Tel.: +91 1762 507084; fax: +91 1762 507085.
E-mail address: singh.sukhbir12@gmail.com (S. Sukhbir).
Peer review under responsibility of King Saud University.

Production and hosting by Elsevier

http://dx.doi.org/10.1016/j.jsps.2015.03.020

Korsmeyer Peppas found excellent kinetics model with release exponent less than 0.45. Chronic constricted injury (CCI) model of optimized NFH-NS in Wistar rats produced significant difference in neuropathic pain behavior ($p < 0.05$) as compared to free NFH over 10 h indicating sustained action. Long term and accelerated stability testing of optimized NFH-NS revealed degradation rate constant 1.695×10^{-4} and shelf-life 621 days at 25 ± 2 °C/60% ± 5% RH.

1. Introduction

Drug delivery is an approach consolidated with dosage form and route of administration. It involves technologies that safely transport an active entity in body to accomplish its anticipated therapeutic outcome. Current efforts in area of drug delivery include development of sustained release formulations in which drug is released over prolonged period of time (Bertrand and Leroux, 2011). Nanospheres are of tremendous scientific significance and have been contemplated as a discovery of novel science to release the drug in a predestined aspect (Buzea et al., 2007). Pain elevates an extensive communal-health obstacle with tremendous upshot on society (Mariana et al., 2010; Breivik et al., 2006).

Neuropathic pain remains one of the most challenging of all neurological diseases which affects millions of people worldwide. It is a chronic condition caused by damage of peripheral nervous system or central nervous system that affects the somatosensory system (Wei et al., 2011; Torrance et al., 2006). Nefopam hydrochloride (NFH) (Fig. 1) is a non-opioid, non-steroidal, centrally acting analgesic drug. It is cyclized analogue of diphenhydramine with its chemical structure similar to orphenadrine (Alfonsi et al., 2004; Podranski et al., 2012). The IUPAC name of NFH is 5-methyl-1-phenyl-1, 3, 4, 6-tetrahydro-2, 5-benzoxazocine hydrochloride and chemical formula is $C_{17}H_{20}ClNO$ (Kyung and Salahadin, 2014).

The inhibition of triple neurotransmitter (serotonin, dopamine and noradrenaline) reuptake produces analgesic effects of NFH (Esposito et al., 1986). The other modes of action may be through histamine H_3 receptors, blockage of voltage-sensitive sodium channels and modulation of glutamatergic transmission (Fuller and Snoddy, 1993; Marazziti et al., 1991). It has been a drug of choice for treatment of postoperative shivering, severe hiccups and neuropathic pain (Girard et al., 2004; Verleye et al., 2004). It has also been useful for relief of dental, musculo-skeletal, acute traumatic, acute wound and cancer pain (Tobin and Gold, 1972; Bolt et al., 1974; Koe, 1976; Cohen, 1974; Klotz, 1974).

The adverse effects of NFH include nausea, vomiting, sweating, dizziness, drowsiness and patient non-compliance due to need of frequent administration. Its usual dose of oral administration is 30–90 mg three to four times daily (Esposito et al., 1986; Marazziti et al., 1991; Fuller and Snoddy, 1993; Girard et al., 2004; Verleye et al., 2004; Tobin and Gold, 1972; Bolt et al., 1974; Koe, 1976; Cohen, 1974; Klotz, 1974). It undergoes extensive hepatic pre-systemic metabolism which is around 83% ± 7. It has oral bioavailability of 30–40% and an elimination half-life near about 3–5 h (Chawla et al., 2003; Aymard et al., 2003).

A modern sustained release dosage form utilizes the drug carriers that ensure prolong drug actions, decrease drug metabolism and reduce drug toxicity. Eudragit (Fig. 2) fulfills these expectations to very high extent (Ana et al., 2007). Eudragit RL 100 and RS 100 are cationic, non-biodegradable, poly (meth) acrylates with quaternary ammonium alkaline group that enables sustained release of the active ingredient by pH-independent swelling. These polymers are insoluble over entire physiological pH range but get swell in the presence of water and digestive fluids due to the presence of ionic group and permeate the drugs slowly by diffusion. Eudragit RL 100 has high permeability while permeability of eudragit RS 100 is low. Consequently, drug release profiles can be altered by blending eudragit RL and eudragit RS in different ratios.

Eudragit RS 100 or RL 100/PLGA nanoparticles loaded with ciprofloxacin have been described previously (Dillen et al., 2006). In present investigation, nefopam hydrochloride-loaded nanospheres (NFH-NS) were synthesized using binary mixture of eudragit RL 100 and RS 100 with sorbitan monooleate as surfactant by quasi solvent diffusion technique. 3^5 Box–Behnken design (BBD) has been applied to analyze the effect of independent variables on dependent variables and to optimize the best possible composition and processing conditions for fabrication of NFH-NS (Gohel and Amin, 1998; Liu et al., 2010; Nazzal and Khan, 2002; Chang et al., 2007; Jifu et al., 2011). It comes into sight to be first to report the fabrication of NFH-NS for antinociception.

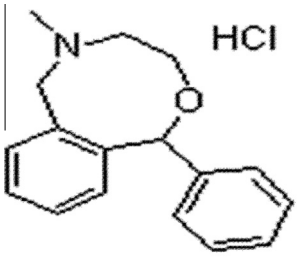

Figure 1 Chemical structure of NFH.

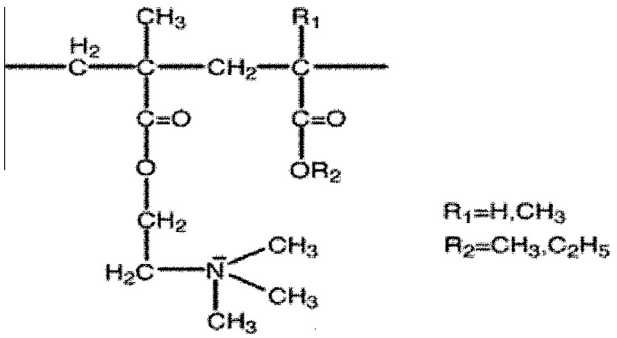

Figure 2 Chemical structure of eudragit.

2. Materials and method

2.1. Materials

Nefopam hydrochloride (5-methyl-1-phenyl-1,3,4,6-tetrahydro-2, 5-benzoxazocine hydrochloride, $C_{17}H_{20}ClNO$, CAS NO-23327-57-3, Mw 289.8 g mol^{-1}, 99.57% purity) was purchased from Hangz Hou-Daying-Chem. Company Ltd., China. Eudragit RL 100 and RS 100 were obtained as a gift sample kindly provided by Evonik Industries AG, Mumbai, India. Heavy liquid paraffin, n-hexane (C_6H_{14}, Mw 86.18) and acetone (2-Propanone, C_3H_6O, Mw 58.08 g mol^{-1}) were obtained from Merck Specialties Private Limited, Mumbai. Magnesium stearate (magnesium octadecanoate, 591.27 g mol^{-1}), span 80 (sorbitan monooleate, HLB-4.3), Potassium dihydrogen phosphate, sodium hydroxide and methanol were procured from Loba Chemicals Private Limited, Mumbai, India. Petroleum ether was procured from Thomas Bakers Chemical Private Limited, Mumbai. All other chemicals used were of analytical grade.

2.2. Methods

2.2.1. Experimental design

In present investigation, 46-run, 5-factor, 3-level Box–Behnken design was utilized for creating second order polynomial models and analyzing quadratic response surface for optimization process using Design-Expert software (Trial Version 9.0.3.1, Stat-Ease Inc., MN). This design can be used to assess main effects, interaction effects and quadratic effects of factors on dependent variables to optimize the formulation. The quadratic model generated by design was

$$\begin{aligned} Y = {} & B_0 + B_1X_1 + B_2X_2 + B_3X_3 + B_4X_4 + B_5X_5 \\ & + B_6X_1X_2 + B_7X_1X_3 + B_8X_1X_4 + B_9X_1X_5 + B_{10}X_2X_3 \\ & + B_{11}X_2X_4 + B_{12}X_2X_5 + B_{13}X_3X_4 + B_{14}X_3X_5 + B_{15}X_4X_5 \\ & + B_{16}X_1^2 + B_{17}X_2^2 + B_{18}X_3^2 + B_{19}X_4^2 + B_{20}X_5^2 \end{aligned} \quad (1)$$

where Y is dependent variable; B_0–B_{20} are regression coefficients of respective independent variables and their interaction terms and X_1, X_2, X_3, X_4, X_5 are independent variables. The terms X_1X_2 and X_i^2 (i = 1, 2 or 3) represent interaction and quadratic terms, respectively (Myers et al., 2009). Factors evaluated in present study were drug/polymer ratio (w/w), surfactant concentration (% w/v), stirring time (h), dispersed phase/continuous phase ratio (DP/CP ratio) (v/v) and stirring speed (rpm) taken at low, medium and high values. Dependent responses were entrapment efficiency (% EE, w/w), mean particle size (nm), process yield (% PY, w/w) and drug loading (% DL, w/w) (Table 1). The design matrix used for experimentation has been presented in Table 2.

Table 2 Box–Behnken experimental design matrix.

Run	X_1	X_2	X_3	X_4	X_5
F1–F4	±1	±1	0	0	0
F5–F8	±1	0	±1	0	0
F9–F12	±1	0	0	±1	0
F13–F16	±1	0	0	0	±1
F17–F20	0	±1	±1	0	0
F21–F24	0	±1	0	±1	0
F25–F28	0	±1	0	0	±1
F29–F32	0	0	±1	±1	0
F33–F36	0	0	±1	0	±1
F37–F40	0	0	0	±1	±1
F41–F46	0	0	0	0	0

2.2.2. Fourier transform infrared spectroscopy (FTIR)

FTIR spectra of NFH, eudragit RL 100, eudragit RS 100, physical mixture and NFH-NS were recorded on FTIR spectrophotometer (IR Affinity-1, Shimadzu, Germany) using IR Solution software. The samples were mixed with potassium bromide powder at 1% and pressed to self-supporting disks. Each spectrum was scanned in the analytical range of 400–4000 cm^{-1}.

2.2.3. Differential scanning calorimetric (DSC)

Thermograms of NFH, eudragit RL 100, eudragit RS 100, physical mixture and NFH-NS were recorded on differential scanning calorimeter (DSC 4000 Perkin Almer, Germany) using Pyris Software. The temperature axis and cell constant of DSC were previously calibrated with indium. A heating rate of 20 °C min^{-1} was employed over a temperature range of 25–350 °C with nitrogen purging (100 mL/min). Samples

Table 1 Variables and their levels in Box–Behnken design.

	Levels		
	−1 (Low)	0 (Medium)	+1 (High)
Independent variables			
X_1 = Drug:polymer ratio (w/w)	1:2	1:3	1:4
X_2 = Surfactant concentration (% w/v)	0.5	1	2
X_3 = Stirring time (hours)	2	3	4
X_4 = [a]DP/CP ratio (v/v)	1:5	1:10	1:15
X_5 = Stirring speed (rpm)	1000	1500	2000
Dependent variables			Constraints
Y_1 = Entrapment efficiency (% EE, w/w)			Maximize
Y_2 = Drug loading (% DL, w/w)			Maximize
Y_3 = Mean particle size (nm)			Minimize
Y_4 = Process yield (% PY, w/w)			Maximize

[a] Dispersed phase/continuous phase.

(2–8 mg) were weighed into an aluminum pan, sealed with pinholes and analyzed by using an empty aluminum pan as reference.

2.2.4. X-ray diffraction (PXRD)

The X-ray diffraction patterns of NFH, eudragit RL 100, eudragit RS 100, physical mixture and NFH-NS were obtained using a specimen of length 10 mm at 25 °C on X-ray diffractometer (X'pert-Pro diffractometer) employing 1.54 A° Cu Kα radiation and 1.39 A° Cu Kβ radiation (tube operated at 45 kV, 40 mA). Data were collected over an angular range from $2\theta = 5°$ to $2\theta = 50°$ in continuous scan mode.

2.2.5. Fabrication of nefopam hydrochloride-loaded nanospheres (NFH-NS)

Nefopam hydrochloride-loaded nanospheres were prepared by quasi solvent diffusion technique (Devarajan and Sonavane, 2007; Jelvehgari et al., 2011). Accurate quantity of NFH, eudragit RL 100 and RS 100 was dissolved in acetone-ethanol mixture. The resultant mixture was extruded slowly through syringe #20 to heavy liquid paraffin containing n-hexane and span 80 which act as hardening agent and an emulsifier, respectively. After stirring for specified time on magnetic stirrer at 38 ± 0.5 °C (REMI, India), nanospheres were collected by centrifugation, and washed four times with petroleum ether succeeded by membrane filtration using 0.22 μm filter. The nanospheres were further collected by ultracentrifugation at 20,000 rpm for 30 min (REMI, India) followed by freeze-drying at −55 °C and 0.5 kPa (vacuum) for 24 h (ISIC Make) in the presence of glucose and lactose as lyoprotectant to obtain fine powder. A schematic representation of Nefopam hydrochloride-loaded nanospheres preparation is illustrated in Fig. 3.

2.3. Evaluation of nanospheres

2.3.1. Entrapment efficiency and drug loading determination

Nanospheres (50 mg) were weighed and extracted with phosphate buffer, pH 7.4 for 24 h and centrifuged at 3500 rpm for 10 min. The supernatant was removed and assayed spectrophotometrically at 266 nm (Systronics AU2701). Each measurement was taken in triplicate (Arindam and Biswanath, 2006). The concentration of dissolved NFH was calculated from calibration curve. The entrapment efficiency (% EE, w/w) and drug loading (% DL, w/w) of nanospheres were calculated according to Eqs. (2) and (3), respectively.

$$\%\text{EE, w/w} = \frac{\text{Weight of drug entrapped}}{\text{Weight of drug}} \times 100 \quad (2)$$

$$\%\text{DL, w/w} = \frac{\text{Weight of drug entrapped}}{\text{Weight of drug} + \text{Weight of polymer}} \times 100 \quad (3)$$

2.3.2. Determination of process yield

Process yield (% PY, w/w) of nanospheres was calculated as the weight of dried nanospheres recovered from each run divided by sum of initial dry weight of starting materials multiplied by hundred (Arica et al., 2005).

2.3.3. Mean particle size analysis

The particle sizes of NFH-NS were measured by optical microscopy using compound microscope (Erma, 23 Tokyo, Japan). All samples were diluted with distilled water before measurement. The particle size measurement was conducted for minimum 300 particles of sample to find out mean particle size.

2.3.4. Optimization and validation

The statistical validation of polynomial equations was entrenched by assessment of statistical parameters such as *p*-value and correlation coefficient (r^2) generated by ANOVA provision available in Design-Expert software. The optimum values of variables were determined by using graphical optimization tool of Design-Expert software based on set constrained criterion of desirability (Myers et al., 2009).

2.3.5. Dynamic light scattering (DLS)

The particle size and polydispersity index (PDI) of optimized batch of NFH-NS were measured by dynamic light scattering (DLS) using zetasizer ver. 7.03 (Nano ZS, Malvern Instruments Ltd., UK). The measurement was taken at 25 °C using disposable sizing cuvette at count rate of 165.6 kcps. Dispersant used was double distilled water having refractive index and viscosity of 1.330 and 0.8872 cP, respectively. The

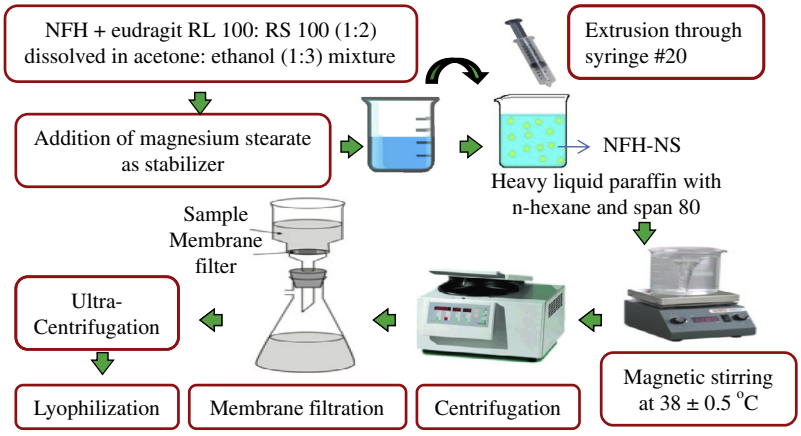

Figure 3 Method for preparation of nefopam hydrochloride-loaded nanospheres.

measurement was taken in triplicate ($n = 3$) after diluting the sample (500×) in dispersant.

2.3.6. Zeta potential (ζ) analysis

The optimized batch of NFH-NS was characterized by zeta potential (ζ) analysis using zetasizer ver. 7.03 (Nano ZS, Malvern Instruments Ltd., UK). The measurement was taken at 25 °C using clear disposable zeta cell at count rate of 29.3 kcps. Dispersant used was double distilled water having refractive index, viscosity and dielectric constant of 1.330, 0.8872 cP and 78.5, respectively. Measurement was carried out after dilution of sample with dispersant to reach a suitable concentration.

2.3.7. Scanning electron microscopy (SEM)

Scanning electron microscopy was performed to assess surface morphology of optimized batch of NFH-NS using a variable pressure scanning electron microscope (Hitachi S3400 N). Nanospheres were plated with gold palladium for 150 s to achieve a 20 nm film under an atmosphere of air (Coater Polaron, 18 mA current at 1.4 kV) and then examined.

2.3.8. In-vitro release study

In-vitro release study was performed using dialysis bag diffusion technique (Singh and Muthu, 2007). Dialysis membrane with a molecular weight cutoff (MWCO) of 12,000–14,000 Da (Himedia, India) was soaked in double distilled water for 12 h prior to experiment (Kathleen et al., 2006). Pure NFH, physical mixture or optimized NFH-NS was placed in dialysis bag containing 50 mL of dissolution medium (phosphate buffer, pH 7.4) at 37 ± 0.5 °C with continuous magnetic stirring at 200 rpm (Remi, India). Two mL sample was withdrawn at specified time intervals for analysis and replenished with equivalent volume of dissolution medium. The amount of NFH in release medium was determined by UV spectrophotometry at 266 nm using double beam UV spectrophotometer (Systronics AU2701, India). Each measurement was taken in triplicate (Arindam and Biswanath, 2006; Barratt, 2000).

2.3.9. Stability studies

Following the ICH guidelines Q1A (R2) and ICH Q1, optimized NFH-NS were stored in stability analysis test chamber (CHM 10S, REMI, India) at 25 ± 2 °C/60 ± 5% RH and 40 ± 2 °C/75 ± 5% RH for conducting long term and accelerated stability testing, respectively. NFH-NS stored at 5 ± 3 °C were treated as control (Madaswamy and Si-Shen, 2009; Mulik et al., 2009). Samples were withdrawn at predetermined time intervals and evaluated for % residual drug content. The plot of log % residual drug content *vs.* time was explored in order to evaluate degradation rate constant (k), half-life ($t_{1/2}$) and shelf-life ($t_{10\%}$) of NFH-NS using Eqs. (4)–(6), respectively.

$$k = 2.303 \times \text{slope} \quad (4)$$

$$t_{1/2} = 0.693/k \quad (5)$$

$$t_{10\%} = 0.152 \times t_{1/2} \quad (6)$$

2.3.10. Neuropathic pain study by chronic constricted injury (CCI) method

2.3.10.1. Surgery. The surgical procedure was performed under ketamine (60 mg/kg) and xylazine (10 mg/kg) anesthesia. The left sciatic nerve was exposed and 4 loose chronic gut ligatures were placed around nerve proximal to the trifurcation. The distance between two adjacent ligatures was 1 mm. The wound was irrigated with saline (0.9% NaCl) and closed in two layers with surgical skin staples.

2.3.10.2. Treatment of injury. Male Wistar rats (180–200 g) were randomly divided into four experimental groups: 1 – phosphate buffer-treated CCI group (control group), 2 – phosphate buffer sham group, 3 – NFH-treated CCI group, and 4 – NFH-NS-treated CCI group. Drugs were administered 30 min before surgery and continued daily to day 14 post-ligation using oral gavage. In order to meet the ethics, behavioral test (cold allodynia) was recorded only on a randomly selected day *i.e.* day 7. Measurements were taken on selected day at predetermined time intervals (0.5 h, 1 h, 2 h, 4 h, 6 h, 8 h and 10 h) after administration of drug to observe the difference in pain behavior of experimental groups.

2.3.10.3. Behavioral test (cold allodynia). The acetone test was used to determine the reactivity to an acetone stimulus. Acetone bubbles were formed at the end of a piece of small polyethylene tubings that was connected to a syringe and bubble was touched to the heel 5 times with an interval of 1 min. Number of paw lift from surface was measured as response. The response was calculated as % paw withdrawal frequency (% PWF) using Eq. (7) as follows:

$$\%\text{PWF} = (\text{Number of paw withdrawal } /5 \text{ Trials}) * 100 \quad (7)$$

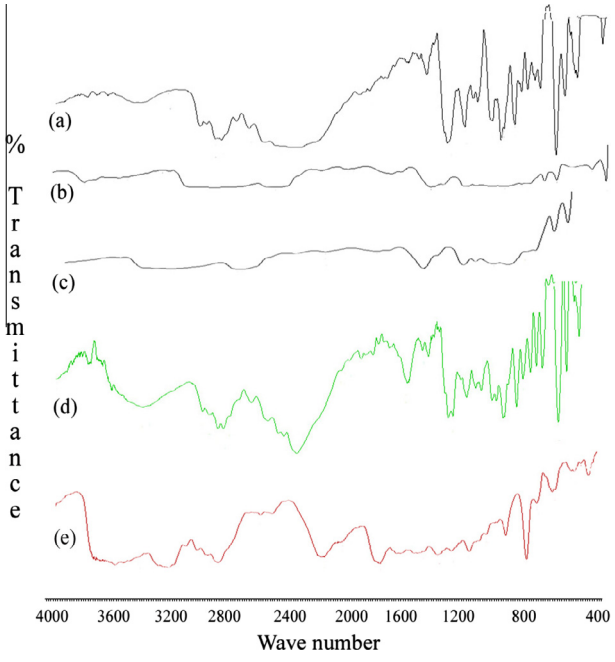

Figure 4 FTIR spectra of (a) NFH, (b) eudragit RL 100, (c) eudragit RS 100, (d) physical mixture and (e) NFH-NS.

2.4. Statistical analysis

All the results were shown as the mean value ± standard deviation. The statistical analysis of polynomial equations was done by ANOVA provision available in Design-Expert software. All other data were analyzed for significance by two way analysis of variance followed by Bonferroni post-test for comparisons among the averages. Statistical difference ($p < 0.05$) was considered significant.

3. Results and discussion

3.1. Fourier transform infrared spectroscopy (FTIR)

The FTIR spectra of NFH, eudragit RL 100, eudragit RS 100, physical mixture and NFH-NS are shown in Fig. 4. The characteristic absorption peaks present in FTIR spectra of NFH at 3429 cm^{-1}, 2910 cm^{-1}, 1446 cm^{-1}, 1346 cm^{-1}, 1024 cm^{-1} and 759 cm^{-1} correspond to C—O—C of cyclic ring, C—H of alkane (s), C=C of aromatic, C—N of amines, C—O stretch and aromatic ring, respectively, and confirm authenticity of drug. The characteristic absorption peaks of NFH remained intact in physical mixture indicated absence of drug–polymer interaction. However, in spectra of NFH-NS, intensity and correlation area of prominent absorption peaks of NFH at 3429 cm^{-1}, 1446 cm^{-1}, 1346 cm^{-1}, 1024 cm^{-1} and 759 cm^{-1} were altered. These findings suggest that weak physical interactions of NFH with eudragit RL 100 and RS 100 take place during nanosphere fabrication.

3.2. Differential scanning calorimetric (DSC)

Differential scanning calorimetry is a rapid and reliable way to screen the incompatibility between drug and polymer and it provides maximum information about possible interactions. Fig. 5 presents DSC curves of (a) NFH, (b) eudragit RL 100, (c) eudragit RS 100, (d) physical mixture and (e) NFH-NS. NFH exhibited a sharp peak at melting temperature (T_f) of 266 °C indicating highly crystalline nature of drug. Eudragit RL 100 and RS 100 showed glass transition temperature (T_g) around 66 °C and 68 °C, respectively, indicating the amorphous nature. The existence of two illustrious endothermic peaks for drug and polymer in physical mixture curve indicates the negligible interaction between drug and polymer. In case of NFH-NS, a deviation toward lower melting temperature (T_f) was detected. This can be explained as NFH and eudragit partially interact to synthesize nanosphere which has different melting point than individual components.

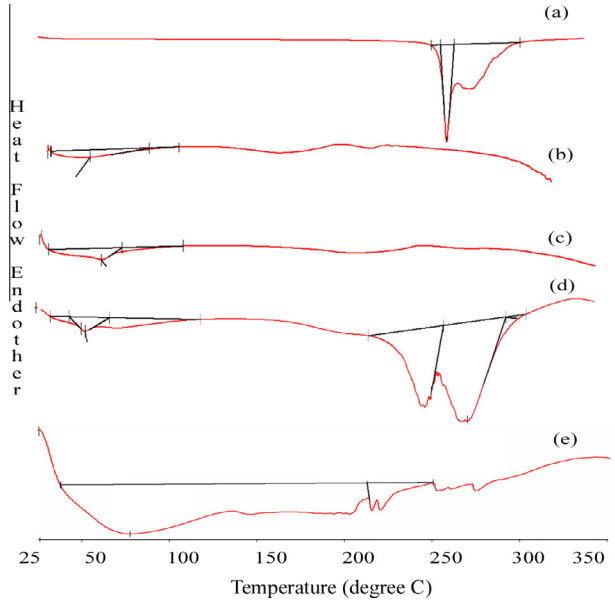

Figure 5 DSC curves of (a) NFH, (b) eudragit RL 100, (c) eudragit RS 100, (d) physical mixture and (e) NFH-NS.

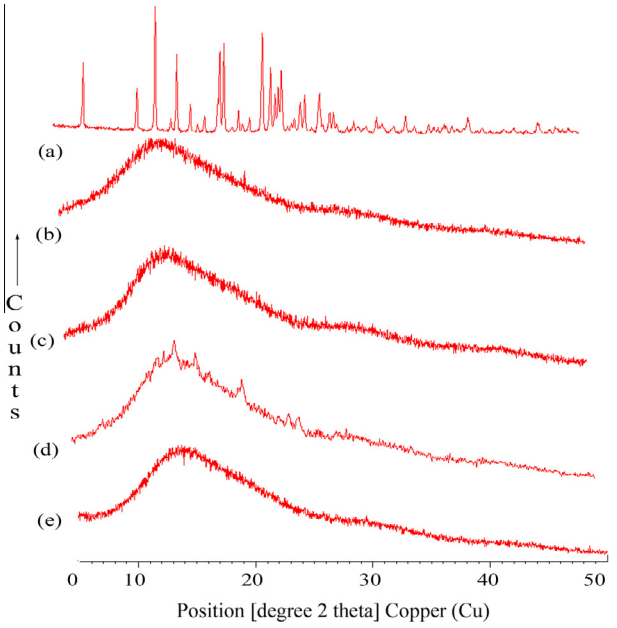

Figure 6 XRD pattern of (a) NFH, (b) eudragit RL 100, (c) eudragit RS 100, (d) physical mixture and (e) NFH-NS.

The DSC curve of NFH-NS shows that original peaks of NFH and eudragit have disappeared. It is evident by comparison of DSC curves that NFH and eudragit exhibit no interactions in physical mixture during formation of nanospheres; NFH and eudragit exhibit some interactions that lead to entrapment of drug in matrix of polymer. The broad peak with onset at 38.52 °C and ending at 213.45 °C indicated that drug was either molecularly dispersed or in amorphous form in matrix of eudragit RL 100 and RS 100 during nanosphere fabrication.

3.3. Powder X-ray diffraction (PXRD)

As shown in Fig. 6a, NFH exhibits sharp crystalline peaks at $2\theta = 7°$, $2\theta = 12°$, $2\theta = 14°$, $2\theta = 15°$, $2\theta = 16°$, $2\theta = 18°$, $2\theta = 19°$, $2\theta = 23°$ and $2\theta = 35°$ indicating highly crystalline behavior of drug. Eudragit RL 100 and RS 100 exhibit negligible peaks in X-ray diffraction pattern indicating amorphous nature of polymers as indicated in Fig. 6b and c, respectively. As depicted in Fig. 6d, crystalline peaks corresponding to NFH at $2\theta = 12°$, $2\theta = 14°$, $2\theta = 15°$, $2\theta = 16°$, $2\theta = 19°$, $2\theta = 23°$ and $2\theta = 35°$ were observed in X-ray diffraction

Table 3 Statistical analysis results of % EE (Y_1), mean particle size (Y_2), % PY (Y_3) and % DL (Y_4).

Parameters	Y_1		Y_2		Y_3		Y_4	
	b_i	p-value	b_i	p-value	b_i	p-value	b_i	p-value
X_1	5.17	< 0.0001*	159.60	< 0.0001	7.94	< 0.0001	−3.06	< 0.0001*
X_2	1.99	0.0047*	−10.79	0.4184	−0.12	0.8507	0.50	0.0040*
X_3	1.09	0.1022	1.14	0.9315	−1.01	0.1147	0.26	0.1065
X_4	2.08	0.0034*	9.52	0.4744	0.88	0.1678	0.53	0.0024*
X_5	3.95	< 0.0001*	−97.14	< 0.0001	1.88	0.0056	0.99	< 0.0001*
X_1X_2	0.11	0.9306	18.23	0.4935	−0.45	0.7144	−0.02	0.9496
X_1X_3	0.81	0.5323	−32.05	0.2333	1.79	0.1603	0.15	0.6362
X_1X_4	−0.06	0.9599	10.30	0.6977	−0.66	0.5981	−0.16	0.6195
X_1X_5	0.32	0.8030	−73.72	0.0096	−1.68	0.1853	−0.07	0.8188
X_2X_3	1.48	0.2599	−14.57	0.5835	0.24	0.8476	0.37	0.2520
X_2X_4	−0.07	0.9552	−37.92	0.1609	1.62	0.2035	−0.02	0.9496
X_2X_5	0.09	0.9445	−28.55	0.2868	0.33	0.7932	0.02	0.9433
X_3X_4	−0.15	0.9106	−31.28	0.2443	−2.03	0.1138	−0.04	0.9057
X_3X_5	1.59	0.2242	−10.85	0.6826	2.52	0.0528	0.40	0.2136
X_4X_5	1.25	0.3370	0.90	0.9730	−0.65	0.6023	0.32	0.3244
X_1^2	−8.33	< 0.0001*	76.41	0.0002	−4.36	< 0.0001	−1.32	< 0.0001*
X_2^2	0.61	0.4895	3.65	0.8389	4.71	< 0.0001	0.16	0.4641
X_3^2	−1.26	0.1576	64.30	0.0014	0.48	0.5722	−0.33	0.1282
X_4^2	−4.33	< 0.0001*	52.73	0.0066	−0.33	0.6958	−1.12	< 0.0001*
X_5^2	−1.22	0.1723	109.41	< 0.0001*	0.42	0.6189	−0.26	0.2366

b_i – Coefficients.
* Significant value $p < 0.01$.

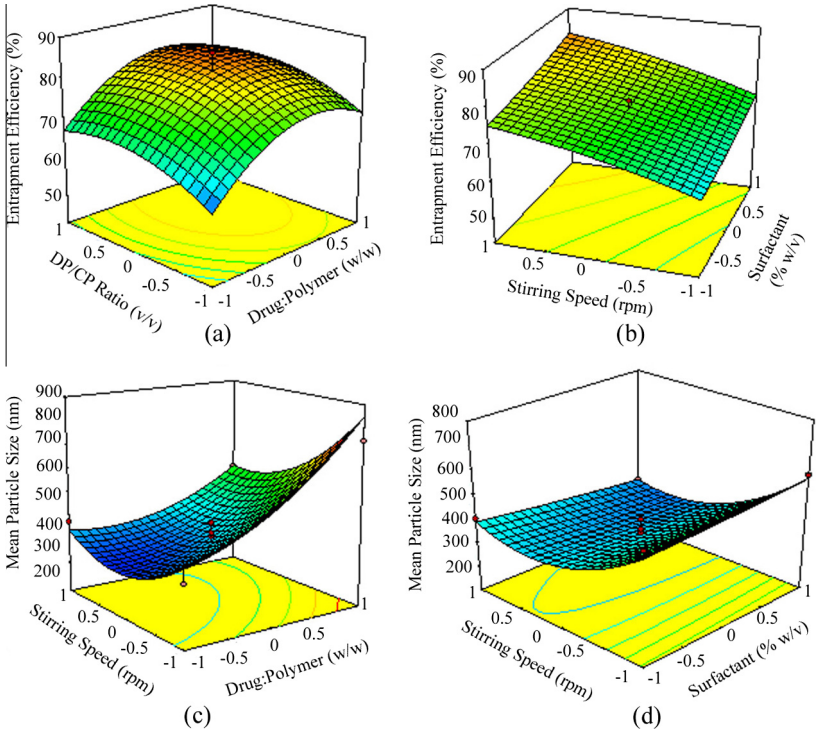

Figure 7 Response surface plot showing effect of (a) drug:polymer ratio and DP/CP ratio on % EE, (b) surfactant and stirring speed on % EE, (c) effect of the drug:polymer ratio and stirring speed on mean particle size and (d) effect of the surfactant and stirring speed on mean particle size.

pattern of physical mixture illustrating insignificant interaction between drug and polymer. In comparison with physical mixture, the crystalline peaks of NFH disappeared in NFH-NS, as observed in Fig. 6e. This suggests that NFH was either molecularly dispersed or in an amorphous form in NFH-NS (Semalty et al., 2009).

3.4. Entrapment efficiency (% EE) (Y_1)

The significant factors affecting % EE (Y_1) were drug/polymer ratio (X_1), surfactant concentration (X_2), DP/CP ratio (X_4) and stirring speed (X_5) ($p < 0.01$, Table 3). The effect can be described by the following quadratic equation:

$$\begin{aligned} Y_1 = {} & 76.49 + 5.17X_1 + 1.99X_2 + 1.09X_3 + 2.08X_4 + 3.95X_5 \\ & + 0.11X_1X_2 + 0.81X_1X_3 - 0.06X_1X_4 + 0.32X_1X_5 \\ & + 1.48X_2X_3 - 0.07X_2X_4 + 0.09X_2X_5 - 0.15X_3X_4 \\ & + 1.59X_3X_5 + 1.25X_4X_5 - 8.33X_1^2 + 0.61X_2^2 - 1.26X_3^2 \\ & - 4.33X_4^2 - 1.22X_5^2 (r^2 = 0.9120) \end{aligned} \quad (8)$$

The value of correlation coefficient (r^2) of Eq. (8) was found to be 0.9120, revealing a good fit. The effect of varying drug/polymer ratio and DP/CP ratio on % EE was examined when stirring speed, surfactant concentration and stirring time were kept constant (Fig. 7a). The result showed that % EE rapidly increased as drug/polymer ratio increased which can be due to greater amount of polymer available to drug to accommodate excessive drugs. Secondly, it can be illustrated by increased viscosity of droplets (Shah and Pathak, 2010; Mao et al., 2008; Jifu et al., 2011). The effect of varying surfactant concentration and stirring speed on % EE was studied when drug/polymer ratio, stirring time and DP/CP ratio were kept constant (Fig. 7b). The entrapment efficacy was significantly increased with increase in surfactant concentration. Probably, this effect was because of tendency of surfactant to stabilize emulsion droplets leading to increased % EE (Ko et al., 2004; Yang et al., 2000).

3.5. Mean particle size analysis

The drug/polymer ratio (X_1) and stirring speed (X_5) had significant positive and negative effects on Y_2 as revealed by positive and negative values of coefficients, respectively, which can be interpreted by the following second-order polynomial quadratic equation:

$$\begin{aligned} Y_2 = {} & 338.30 + 159.60X_1 - 10.79X_2 + 1.14X_3 + 9.52X_4 \\ & - 97.14X_5 + 18.23X_1X_2 - 32.05X_1X_3 + 10.30X_1X_4 \\ & - 73.72X_1X_5 - 14.57X_2X_3 - 37.92X_2X_4 - 28.55X_2X_5 \\ & - 31.28X_3X_4 - 10.85X_3X_5 + 0.90X_4X_5 + 76.41X_1^2 \\ & + 3.65X_2^2 + 64.30X_3^2 + 52.73X_4^2 + 109.41X_5^2 (r^2 = 0.9195) \end{aligned} \quad (9)$$

The effect of varying drug/polymer ratio and stirring speed on mean particle size (Y_2) was studied when surfactant concentration, stirring time and DP/CP ratio were kept constant (Fig. 7c). It was noted that increase in stirring speed results in remarkable decrease in mean particle size which can be explained as force exerted due to high rpm results in reduction in particle size. It has also been demonstrated that mean particle size increased rapidly with increasing drug/polymer ratio which can be illustrated by increase in density of dispersed phase and size of droplets (Shah and Pathak, 2010; Mao et al., 2008; Jifu et al., 2011). In Fig. 7d, the effect of varying surfactant concentration and stirring speed on the mean particle size (Y_2) was studied when the drug/polymer ratio, stirring

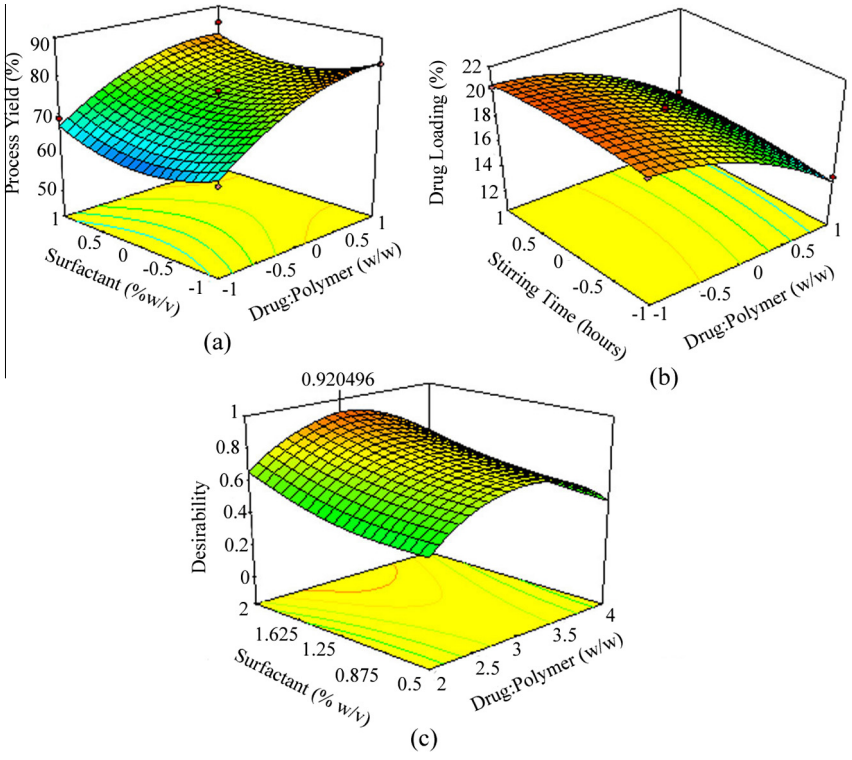

Figure 8 Response surface plot showing effect of (a) drug:polymer ratio and surfactant on % PY, (b) effect of the drug:polymer ratio and stirring time on % DL and (c) response graph for desirability function of optimized NFH-NS.

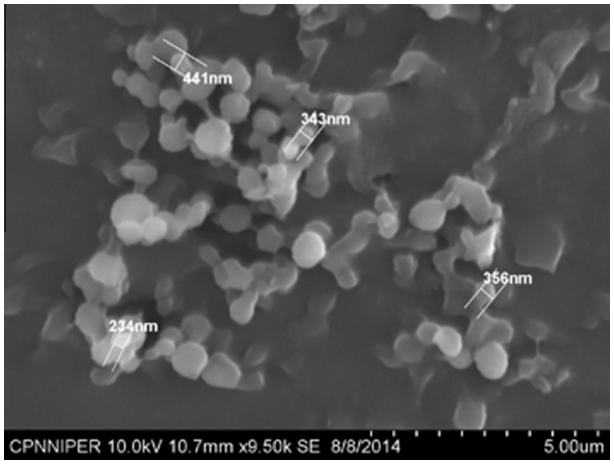

Figure 9 Scanning electron micrographs of optimized NFH-NS fabricated with 1:3 drug:polymer ratio, 2% surfactant concentration, 1:12 DP/CP ratio, 2000 rpm stirring speed, 3.8 h stirring time (×9500).

time and DP/CP ratio were kept constant. It was noted that the increase in surfactant concentration could efficiently reduce the particle size of nanospheres due to the surfactant-induced reduction in surface tension between the DP and CP. In addition, surfactant helps to stabilize the newly generated surfaces and prevents particle aggregation (Gullapalli and Sheth, 1999; Ko et al., 2004; Yang et al., 2000; Jifu et al., 2011; Hamed and Sakr, 2001).

3.6. Process yield (% PY)

Results in Table 3 signify that the independent factors affecting the % PY were the drug/polymer ratio (X_1) and stirring speed (X_5) ($p < 0.01$). The effect can be elucidated by the following polynomial quadratic equation:

$$\begin{aligned} Y_3 = {} & 74.70 + 7.94X_1 - 0.12X_2 - 1.01X_3 + 0.88X_4 \\ & + 1.88X_5 - 0.46X_1X_2 + 1.79X_1X_3 - 0.66X_1X_4 \\ & - 1.68X_1X_5 + 0.24X_2X_3 + 1.61X_2X_4 + 0.33X_2X_5 \\ & - 2.03X_3X_4 + 2.52X_3X_5 - 0.65X_4X_5 - 4.37X_1^2 \\ & + 4.71X_2^2 + 0.48X_3^2 - 0.33X_4^2 + 0.42X_5^2 (r^2 = 0.9195) \quad (10) \end{aligned}$$

The main effects of X_1, X_2, X_3, X_4 and X_5 represent the average result of changing 1 variable at a time from its low level to its high level. The negative and positive coefficients before independent variables pinpoint negative and positive effect on the % PY, respectively. The interaction terms (X_1X_2, X_1X_3, X_1X_4, X_1X_5, X_2X_3, X_2X_4, X_2X_5, X_3X_4, X_3X_5 and X_4X_5) show how the % PY changes when 2 variables are simultaneously changed. Analyzing these coefficients in the above second order polynomial mode shows how the increase of drug/polymer ratio (X_1) and stirring speed (X_5) enhances the % PY (Lee et al., 2000). The value of the correlation coefficient (r^2) of Eq. (6) was found to be 0.9195, indicating a good fit. The effect of varying the drug/polymer ratio and surfactant concentration on % PY was demonstrated when stirring time, stirring speed and DP/CP ratio were kept constant (Fig. 8a). The result showed that % PY increased rapidly with increasing drug/polymer ratio which can be illustrated by the increase in total weight nanospheres recovered (Shah and Pathak, 2010; Mao et al., 2008; Jifu et al., 2011).

3.7. Drug loading (% DL)

The % DL was significantly influenced by the drug/polymer ratio (X_1), surfactant concentration (X_2), DP/CP ratio (X_4) and stirring speed (X_5) ($p < 0.01$), Table 3. The effect can be annotated by the following quadratic equation:

$$\begin{aligned} Y_4 = {} & 19.12 - 3.06X_1 + 0.5X_2 + 0.26X_3 + 0.53X_4 \\ & + 0.99X_5 - 0.02X_1X_2 + 0.15X_1X_3 - 0.16X_1X_4 \\ & - 0.07X_1X_5 + 0.37X_2X_3 - 0.02X_2X_4 + 0.02X_2X_5 \\ & - 0.04X_3X_4 + 0.40X_3X_5 + 0.32X_4X_5 - 1.32X_1^2 \\ & + 0.16X_2^2 - 0.33X_3^2 - 1.12X_4^2 - 0.26X_5^2 (r^2 = 0.9556) \quad (11) \end{aligned}$$

The value of the correlation coefficient (r^2) of Eq. (7) was found to be 0.9556, attributing a good fit. The effect of changing the drug/polymer ratio and stirring time on the % DL was studied when the surfactant concentration, DP/CP ratio and stirring speed were kept constant (Fig. 8b). The drug/polymer ratio had a significant and negative effect on % DL as specified by the negative value in the quadratic equation (Shah and Pathak, 2010; Mao et al., 2008; Jifu et al., 2011; Ko et al., 2004; Yang et al., 2000).

3.8. Optimization and validation

The desirability function was explored using Design-Expert software to achieve the optimized formulation. The optimum formulation was established on the set paradigm of maximum % EE, minimum mean particle size, maximum % PY and maximum % DL. Consequently, an additional batch of NFH-NS with predicted levels of factors was produced to authenticate persuasiveness of the optimization strategy. The composition and processing conditions for optimized formulation were 1:3 drug/polymer ratios (w/w), 2% (w/v) surfactant, 3.8 h stirring time, 1:12 DP/CP ratio and 2000 rpm stirring speed, which accomplish the prerequisite of optimization. Desirability function for optimized formulation was found to be 0.920 (Fig. 8c). The optimized formulation has 84.972 ± 1.23% % EE, mean particle size of 328.366 nm ± 4.23, % PY of 83.60 ± 3.23% and 21.41 ± 2.02% % DL, which were in compliance with the predicted values.

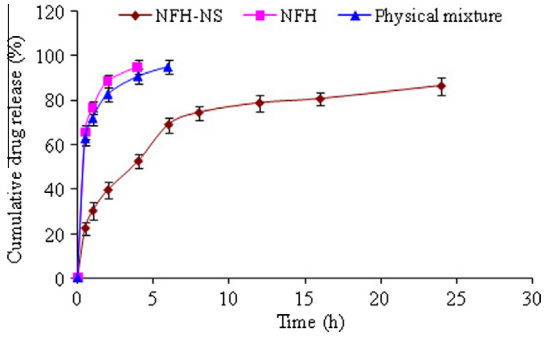

Figure 10 *In-vitro* drug release profile of nefopam hydrochloride from optimized batch of NFH-NS, physical mixture and pure drug in phosphate buffer (pH 7.4) at 37 ± 0.5 °C.

Table 4 *In-vitro* drug release data of optimized NFH-NS for various release kinetic models.

Order	R^2	*a*	*b*	Regression equation	*k*	*n*
Zero	0.844	3.022	30.69	$y = 3.022x + 30.69$	3.022 (h^{-1})	–
First	0.969	−0.038	1.879	$y = -0.038x + 1.879$	−0.038 (h^{-1})	–
Higuchi	0.961	18.02	9.807	$y = 18.02x + 9.807$	18.02 ($h^{-1/2}$)	–
Peppas	0.988	0.425	1.409	$y = 0.425x + 1.409$	25.8 (h^{-n})	0.425
Hixon–Crowell	0.935	−0.093	3.122	$y = -0.093x + 4.165$	−0.093 ($h^{-1/3}$)	–

R^2 – Squared correlation coefficient; *a* – Slope; *b* – Intercept; *k* – Release constant; *n* – Release exponent of Korsmeyer–Peppas model.

3.9. Dynamic light scattering (DLS)

DLS was performed to characterize the mean particle size (*z*-average) and polydispersity index (PDI) of optimized NFH-NS for evaluation of particle size distribution. *Z*-average and polydispersity index of nanospheres were found to be 648 ± 4.8 nm and 0.53, respectively. The data indicated a high degree of homogeneity with a relatively narrow particle size distribution of NFH-NS in nanometric range.

3.10. Zeta potential analysis

Zeta potential (ζ) valuates overall surface charge attained by particles in a particular medium of the colloidal system and is explored as one of the paradigms of stability of colloidal system. It is influenced by the composition of particle and medium in which it is dispersed. Nanospheres with a zeta potential above (±) 30 mV have been researched to be stable in colloidal system, as the surface charge prevents aggregation of particles due to stronger repulsive interactions among particles (Jifu et al., 2011; Rahman et al., 2010). In present study, the zeta potential value of optimized NFH-NS was +4.48 mV. The absolute value of zeta potential was lower than those values reported in the literature. This might be attributed to sorbitan monooleate, a nonionic surfactant which decreases the electrostatic repulsion between the particles and sterically stabilizes the nanospheres by forming a coat around their surface (Schwarz et al., 1994). The positive charge of NFH-NS may be attributed from cationic poly (meth) acrylates, *viz*. eudragit RL 100 and RS 100, having quaternary ammonium group.

3.11. Scanning electron microscopy

SEM studies had been used to determine texture and examine surface morphology of optimized NFH-NS. Scanning electron micrographs affirmed that nanospheres were almost spherical in shape with smooth morphology (Fig. 9).

3.12. In-vitro drug release behavior

NFH rendered a rapid release of 95% of drug within 6 h, whereas optimized NFH-NS revealed a biphasic pattern with a burst release during first 4 h, succeeded by a sustained release over 24 h (Fig. 10). The initiatory fast release of drug from nanospheres could be described by drug desorption from larger outer specific surface of nanosphere. The mechanism of drug release was resolved by finding R^2 value for various kinetic models *viz*. first-orders, Higuchi, Korsmeyer–Peppas and Hixon–Crowell (Table 4). It was found that Korsmeyer–Peppas model was excellent ($y = 0.425x + 1.409$, $R^2 = 0.9888$). The '*n*' value was found to be 0.425 which was less than 0.45 illustrating drug release rate was dominated by Fickian diffusion from polymer matrix (Peppas and Sahlin, 1989; Paulo and José Manuel, 2001; Das and Das, 1998).

3.13. Stability study

Long term and accelerated stability testing of optimized NFH-NS was conducted to evaluate degradation rate constant (*k*), half-life ($t_{1/2}$) and shelf-life ($t_{10\%}$) of NFH-NS at 25 ± 2 °C/60 ± 5% RH and 40 ± 2 °C/75 ± 5% RH, respectively. Degradation rate constant (*k*) was estimated from plot of log

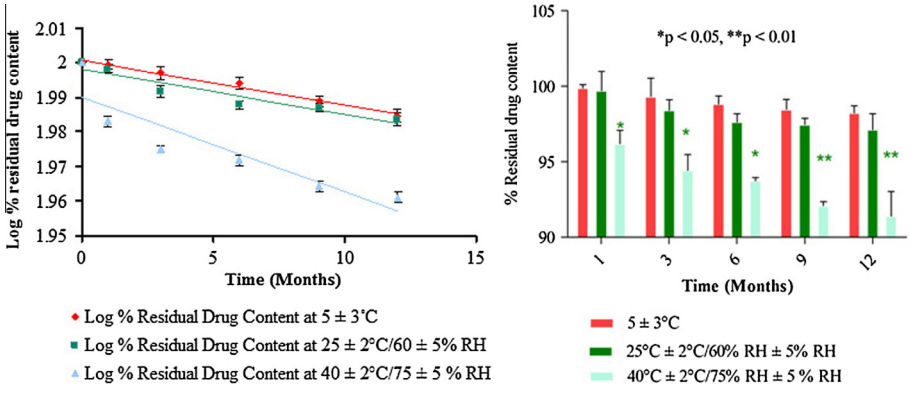

Figure 11 Stability of optimized NFH-NS on storage under various temperatures and % RH condition (a) log % residual drug content and (b) % residual drug content.

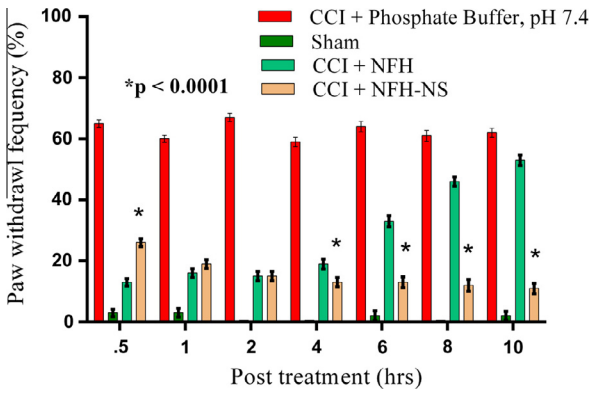

Figure 12 The frequency of paw withdrawal in response to acetone at several time points post treatment in phosphate buffer-treated CCI group, phosphate buffer-treated sham group, NFH-treated CCI group and NFH-NS-treated CCI group. Results are expressed as the mean ± SEM of 6 animals per group. Asterisks indicate a significant difference between treated groups compared with control group ($^{*}p < 0.0001$).

% residual drug content *vs.* time (Fig. 11a). It was found that NFH-NS stored at 25 ± 2 °C/60 ± 5% RH and 40 ± 2 °C/75 ± 5% RH have degradation rate constant (k) of 1.695×10^{-4} which corresponds to $t_{10\%}$ value of nearly 621 days and 2.0615×10^{-4} which corresponds to $t_{10\%}$ value of nearly 510 days. After 12 months of storage of NFH-NS at 25 ± 2 °C/60 ± 5% RH, the significant difference in % residual drug content was not observed as compared to control (Fig. 11b). These findings revealed that the remarkable stability of NFH-NS was achieved at 25 ± 2 °C/60 ± 5% RH.

3.14. Chronic constricted injury (CCI) method

Neuropathic pain study was performed by chronic constricted injury (CCI) method to compare pure NFH and optimized NFH-NS by cold allodynia. NFH-NS-treated CCI group exhibits no significant difference in pain behavior till 2 h of drug administration as compared to NFH-treated CCI group ($p > 0.05$) (Fig. 12). After 2 h, NFH-NS-treated CCI group produces significant difference in pain behavior till 10 h of drug administration as compared to NFH-treated CCI group indicating sustained release of drug from NFH-NS ($p < 0.0001$).

4. Conclusions

This research work might provide yardstick for potential use of eudragit polymers for synthesis of NFH-NS. In current investigation, NFH-NS with high drug entrapment efficiency and drug loading were successfully synthesized using eudragit RL 100 and RS 100 by a simple and inexpensive quasi solvent diffusion technique and optimized by Box–Behnken design. The present study conclusively manifested that the optimal formulation of NFH-NS having desirability function 0.920 was achieved with 1:3 drug/polymer ratios (w/w), 2% (w/v) sorbitan monooleate as surfactant, 3.8 h stirring time, 1:12 DP/CP ratio and 2000 rpm stirring speed. The optimized NFH-NS followed biphasic Fickian diffusional release pattern from polymer matrix and exhibited the requisite stability at 25 ± 2 °C/60 ± 5% RH. Chronic constricted injury (CCI) model in Wistar rats manifested sustained action of optimized NFH-NS. It was concluded that NFH-NS could substantially be utilized for sustained drug delivery.

Acknowledgments

The authors wish to thank Evonik Industries AG, Mumbai, India, for providing eudragit RL 100 and RS 100 as a kind gift sample and Chitkara University for infrastructural support to carry out this work. The authors are grateful to Punjab Technical University for providing access to Science Direct and anti-plagiarism software.

References

Alfonsi, P., Adam, F., Passard, A., Guignard, B., Sessler, D.I., Chauvin, M., 2004. Nefopam- a non-sedative benzoxazocine analgesic selectively reduces the shivering threshold in unanesthetized subjects. Anesthesiology 100, 37–43.

Ana, R.C.D., Christelle, R., Arlette, V.G., Catarina, M.M.D., Pascale, S.P., 2007. Preparation of acetazolamide composite microparticles by supercritical anti-solvent techniques. Int. J. Pharm. 332, 132–139.

Arica, B., Kas, H.S., Moghdam, A., Akalan, N., Hincal, A.A., 2005. Carbidopa/levodopa-loaded biodegradable microspheres: *in-vivo* evaluation on experimental parkinsonism in rats. J. Control. Release 102, 689–697.

Arindam, H., Biswanath, S., 2006. Preparation and *in vitro* evaluation of polystyrene-coated (PS-coated) microcapsule of drug–resin complex for achieving prolonged release of diltiazem hydrochloride. AAPS PharmSciTech 7, 34–49.

Aymard, G., Warot, D., Demolis, P., 2003. Comparative pharmacokinetics and pharmacodynamics of intravenous and oral nefopam in healthy volunteers. Pharmacol. Toxicol. 92, 279–286.

Barratt, G.M., 2000. Therapeutic applications of colloidal drug carriers. Pharm. Sci. Technol. Today 3, 163–171.

Bertrand, N., Leroux, J.C., 2011. The journey of a drug carrier in the body: an anatomo-physiological perspective. J. Control. Release 161, 152–163.

Bolt, A.G., Graham, G., Wilson, P., 1974. Stereoselective demethylation of the enantiomers of nefopam, an experimental antidepressant and skeletal muscle relaxant. Xenobiotica 4, 355–363.

Breivik, H., Collett, B., Ventafridda, V., Cohen, R., Gallacher, D., 2006. Survey of chronic pain in Europe: prevalence, impact on daily life, and treatment. Eur. J. Pain 10, 287–333.

Buzea, C., Pacheco, I.I., Robbie, K., 2007. Nanomaterials and nanoparticles: sources and toxicity. Biointerphases 2, 17–71.

Chang, J., Huang, Y., Hou, S., Wang, R., Wu, P., Tsai, Y., 2007. Formulation optimization of meloxicam sodium gel using response surface methodology. Int. J. Pharm. 338, 48–54.

Chawla, J., Le Guern, M.E., Alquier, C., Kalhorn, T.F., Levy, R.H., 2003. Effect of route of administration on the pharmacokinetic behavior of enantiomers of nefopam and desmethylnefopam. Ther. Drug Monit. 25, 203–210.

Cohen, A., 1974. Nefopam hydrochloride for pain relief. Curr. Ther. Res. Clin. Exp. 16, 184–193.

Das, S.K., Das, N.G., 1998. Preparation and *in-vitro* dissolution profile of dual polymer eudragit RS 100 and RL 100 microparticles of diltiazem hydrochloride. J. Microencapsul. 15, 445–452.

Devarajan, Padma V., Sonavane, Ganeshchandra S., 2007. Preparation and *in-vitro/in-vivo* evaluation of gliclazide loaded eudragit nanoparticles as sustained release carriers. Drug. Dev. Ind. Pharm. 33, 101–111.

Dillen, K., Vandervoort, J., Van den, M.G., Ludwig, A., 2006. Evaluation of ciprofloxacin-loaded eudragit RS100 or RL100/PLGA nanoparticles. Int. J. Pharm. 314, 72–82.

Esposito, E., Romandini, S., Merlo-Pich, E., Mennini, T., Samanin, R., 1986. Evidence of the involvement of dopamine in the analgesic effect of nefopam. Eur. J. Pharmacol. 128, 157–164.

Fuller, R.W., Snoddy, H.D., 1993. Evaluation of nefopam as a monoamine uptake inhibitor *in-vivo* in mice. Neuropharmacology 32, 995–999.

Girard, P., Pansart, Y., Coppé, M.C., Verniers, D., Gillardin, J.M., 2004. Role of the histamine system in nefopam-induced antinociception in mice. Eur. J. Pharmacol. 503, 63–69.

Gohel, M., Amin, A., 1998. Formulation optimization of controlled release diclofenac sodium microspheres using factorial design. J. Control. Release 51, 115–122.

Gullapalli, R., Sheth, B., 1999. Influence of an optimized non-ionic emulsifier blend on properties of oil-in-water emulsions. Eur. J. Pharm. Biopharm. 48, 233–238.

Hamed, E., Sakr, A., 2001. Application of multiple response optimization technique to extended release formulations design. J. Control. Release 73, 329–338.

Jelvehgari, M., Barar, J., Valizadeh, H., Shadrou, S., Nokhodchi, A., 2011. Formulation, characterization and *in-vitro* evaluation of theophylline-loaded eudragit RS 100 microspheres prepared by an emulsion-solvent diffusion/evaporation technique. http://www.ncbi.nlm.nih.gov/pubmed/20722498 Pharm. Dev. Technol. 16, 637–644.

Jifu, H., Xinsheng, F., Yanfang, Z., Jianzhu, W., Fengguang, G., Fei Li, X.P., 2011. Development and optimization of solid lipid nanoparticle formulation for ophthalmic delivery of chloramphenicol using a Box–Behnken design. Int. J. Nanomed. 6, 683–692.

Kathleen, D., Jo, V., Guy, V.M., Annick, L., 2006. Evaluation of ciprofloxacin-loaded Eudragit® RS100 or RL100/PLGA nanoparticles. Int. J. Pharm. 314, 72–82.

Klotz, A.L., 1974. Long-term safety of nefopam hydrochloride (acupan), a new analgesic formulation. Curr. Ther. Res. Clin. Exp. 16, 602–608.

Ko, J.A., Park, H.J., Park, Y.S., Hwang, S.J., Park, J.B., 2004. Chitosan microparticle preparation for controlled drug release by response surface methodology. J. Microencapsul. 20, 791–797.

Koe, B.K., 1976. Molecular geometry of inhibitors of the uptake of catecholamine's and serotonin in synaptosomal preparations of rat brain. J. Pharmacol. Exp. Ther. 199, 649–661.

Kyung, H.K., Salahadin, A., 2014. Rediscovery of nefopam for the treatment of neuropathic pain. Korean J. Pain 27, 103–111.

Lee, J.H., Park, T.G., Choi, H.K., 2000. Effect of formulation and processing variables on the characteristics of microspheres for water soluble drugs prepared by w/o/o double emulsion solvent diffusion method. Int. J. Pharm. 196, 75–83.

Liu, C., Wu, C., Fang, J., 2010. Characterization and formulation optimization of solid lipid nanoparticles in vitamin K1 delivery. Drug Dev. Ind. Pharm. 36, 751–761.

Madaswamy, S.M., Si-Shen, F., 2009. Pharmaceutical stability aspects of nanomedicines. Nanomedicines 4, 857–860.

Mao, S., Shi, Y., Li, L., Xu, J., Schaper, A., Kissel, T., 2008. Effects of process and formulation parameters on characteristics and internal morphology of poly (D, L-lactide-co-glycolide) microspheres formed by the solvent evaporation method. Eur. J. Pharm. Biopharm. 68, 214–223.

Marazziti, D., Rotondo, A., Ambrogi, F., Cassano, G.B., 1991. Analgesia by nefopam: does it act through serotonin. Drugs Exp. Clin. Res. 17, 259–261.

Mariana, S., Catalina, R.B., Muhammad, F.A., Kurt, S., Helmut, S., 2010. *In-vitro* and *in-vivo* pharmacological profile of the 5-benzyl analogue of 14-methoxymetopon, a novel opioid analgesic with reduced propensity to alter motor function. Eur. J. Pharm. Sci. 41, 125–135.

Mulik, R., Mahadik, K., Paradkar, A., 2009. Development of curcuminoids loaded poly (butyl) cyanoacrylates nanoparticles: physicochemical characterization and stability study. Eur. J. Pharm. Biopharm. 37, 395–404.

Myers, R.H., Montgomery, D.C., Anderson-Cook, C.M., 2009. Response Surface Methodology: Process and Product Optimization Using Designed Experiments, third ed. John Wiley & Sons, New York.

Nazzal, S., Khan, M., 2002. Response surface methodology for the optimization of ubiquinone self-nanoemulsified drug delivery system. AAPS PharmSciTech 3, 23–31.

Paulo, C., José Manuel, S.L., 2001. Modeling and comparison of dissolution profiles. Eur. J. Pharm. Sci. 13, 123–133.

Peppas, N.A., Sahlin, J.J., 1989. A simple equation for the description of solute release. III. Coupling of diffusion and relaxation. Int. J. Pharm. 57, 169–172.

Podranski, T., Bouillon, T.W., Riva, T., Kurz, A.M., Oehmke, M.J., 2012. Compartmental pharmacokinetics of nefopam during mild hypothermia. Br. J. Anaesth. 108, 784–791.

Rahman, Z., Zidan, A., Habib, M., Khan, M., 2010. Understanding the quality of protein loaded PLGA nanoparticles variability by Plackett–Burman design. Int. J. Pharm. 389, 186–194.

Schwarz, C., Mehnert, W., Lucks, J., Müller, R., 1994. Solid lipid nanoparticles (SLN) for controlled drug delivery. I. Production, characterization and sterilization. J. Control. Release 30, 83–96.

Semalty, A., Semalty, M., Singh, D., Rawat, M.S., 2009. Development and physicochemical evaluation of pharmacosomes of diclofenac. Acta Pharm. 59, 335–344.

Shah, M., Pathak, K., 2010. Development and statistical optimization of solid lipid nanoparticles of simvastatin by using 2^3 full-factorial designs. AAPS PharmSciTech 11, 489–496.

Singh, S., Muthu, M.S., 2007. Studies on biodegradable polymeric nanoparticles of risperidone: *In vitro* and *in-vivo* evaluation. Nanomedicine 3, 305–319.

Tobin, W.E., Gold, R.H., 1972. Nefopam hydrochloride: a novel muscle relaxant. J. Clin. Pharmacol. New Drugs 12, 230–238.

Torrance, N., Smith, B.H., Bennett, M.I., Lee, A.J., 2006. The epidemiology of chronic pain of predominantly neuropathic origin. Results from a general population survey. J. Pain 7, 281–289.

Verleye, M., André, N., Heulard, I., Gillardin, J.M., 2004. Nefopam blocks voltage-sensitive sodium channels and modulates glutamatergic transmission in rodent. Brain Res. 1013, 249–255.

Wei, W., Jianguo, G., Yun-Qing, L., Yuan-Xiang, T., 2011. Are voltage-gated sodium channels on the dorsal root ganglion involved in the development of neuropathic pain? Mol. Pain 7, 16–25.

Yang, Y., Chung, T., Bai, X., Chan, W., 2000. Effect of preparation conditions on morphology and release profiles of biodegradable polymeric microspheres containing protein fabricated by double-emulsion method. Chem. Eng. Sci. 55, 2223–2236.